Catal Surv Asia (2008) 12:170–183
DOI 10.1007/s10563-008-9049-1

Fischer–Tropsch Synthesis by Carbon Dioxide Hydrogenation on Fe-Based Catalysts

P. S. Sai Prasad · Jong Wook Bae · Ki-Won Jun · Kyu-Wan Lee

Published online: 10 September 2008

Abstract Impregnated and co-precipitated, promoted and unpromoted, bulk and supported iron catalysts were prepared, characterized, and subjected to hydrogenation of CO_2 at various pressures (1–2 MPa) and temperatures (573–673 K). Potassium, as an important promoter, enhanced the CO_2 uptake and selectivity towards olefins and long-chain hydrocarbons. Al_2O_3, when added as a structural promoter during co-precipitation, increased CO_2 conversion as well as selectivity to C_{2+} hydrocarbons. Among V, Cr, Mn and Zn promoters, Zn offered the highest selectivity to C_2–C_4 alkenes. The different episodes involved in the transformation of the catalyst before it reached steady-state were identified, on the co-precipitated catalyst. Using a biomass derived syngas ($CO/CO_2/H_2$), CO alone took part in hydrogenation. When enriched with H_2, CO_2 was also converted to hydrocarbons. The deactivation of impregnated Fe–K/Al_2O_3 catalyst was found to be due to carbon deposition, whereas that for the precipitated catalyst was due to increase in crystallinity of iron species. The suitability of SiO_2, TiO_2, Al_2O_3, HY and ion exchanged NaY as supports was examined for obtaining high activity and selectivity towards light olefins and C_{2+} hydrocarbons and found Al_2O_3 to be the best support. A comparative study with Co catalysts revealed the advantages of Fe catalysts for hydrocarbon production by F–T synthesis.

Keywords Iron catalysts · F–T synthesis · Carbon dioxide hydrogenation · Hydrocarbons

P. S. Sai Prasad · J. W. Bae · K.-W. Jun (✉) · K.-W. Lee
Alternative Chemicals/Fuel Research Center, Korea Research Institute of Chemical Technology (KRICT), P.O. Box 107, Yuseong, Daejeon 305-600, South Korea
e-mail: kwjun@krict.re.kr

1 Introduction

The world's energy sector is confronted with two important problems; one being the sky rocketing prices of petroleum products and the second, the increasing amount of carbon dioxide liberated into the atmosphere from the power plants leading to global warming. Therefore, it is necessary to identify methodologies for the development of alternate sources of energy, at the same time prevent carbon dioxide reaching the atmosphere. It is in this context that the transformation of carbon dioxide into useful products has gained enormous attention. The hydrogenation of carbon dioxide into different products is gaining importance as valuable chemicals can be produced from an unlimited source, even though this methodology is subjected to criticism that the normal sources of hydrogen (excepting solar and nuclear) again involve carbon dioxide liberation and the common products like methanol and methane may not be that valuable [1]. However, the enormous scope for the production of industrial feed stocks such as lower olefins and long chain branched hydrocarbons has been the greatest impetus for the extensive research in the development of technologies for hydrogenation of carbon dioxide. Production of syngas from coal or biomass involves generation of significant quantities of CO_2. At present, the hydrocarbon synthesis processes adopt separation of CO_2 from the feed streams (ex. Rectisol process). However, CO_2 hydrogenation can be employed to convert CO_2 stream from oxy-fuel combustion as well as excess CO_2 from biomass gasification when cheap hydrogen becomes available.

A number of studies have been published on CO_2 hydrogenation to hydrocarbons. Primarily, these can be divided into two categories: the methanol mediated and the non-methanol mediated [2, 3]. In the methanol mediated

hydrocarbon synthesis carbon dioxide and hydrogen react on Cu–Zn based catalysts to produce methanol which is subsequently transformed into other hydrocarbons like gasoline (by MTG process), dimethyl ether, etc., However, in spite of considerable efforts made in the development of composite catalysts, this method usually gives light alkanes as major hydrocarbon products because the methanol synthesis catalyst further hydrogenates the alkenes [4]. In the case of non-methanol mediated processes CO_2 hydrogenation proceeds by two steps; namely the reverse water gas (RWGS) shift and the Fischer–Tropsch (F–T) synthesis. There are also references in the literature indicating the possibility for direct hydrocarbon synthesis from CO_2 and H_2 [5].

A number of transition group elements have been tried to interact with carbon dioxide. Omae [6] has nicely brought out the details on these interactions and the production of various compounds like formic acid and its esters, formamides and other hydrogenation products. However, when it comes to F–T synthesis from CO_2 and H_2, iron oxides have been used very extensively. Iron oxides are active in both water gas shift and reverse water gas shift reactions [7] and they are adjudged as the ideal catalysts for the F–T synthesis of CO_2-containing syngas feeds [8, 9]. The importance of these catalysts arises from the olefinic nature of the obtained products which are used as feed stocks for chemical industry. The products are also of high specific value as they are cleaner (no sulfur, no aromatics) than the petroproducts. However, when used alone, iron catalysts offer high selectivity to non-desired products such as methane. They also undergo rapid deactivation. In order to make them active, selective and stable several promoters and stabilizers are used. CO_2 hydrogenation has been carried out on bulk as well as supported multi-component catalyst systems.

The active phase of the catalyst is believed to be the iron carbide species, while the contribution by iron oxide/metallic iron is also being investigated. Miller and Moskovits [10] showed a different pathway for the formation of oxygenates implying that other active phases may also exist on the surface of the catalyst. It is very difficult to pin point the nature of active phase as the iron based catalysts change their phases during the reaction from the Fe_2O_3 to Fe_3O_4 and from there to metallic Fe to iron carbides. The final active site depends upon the nature of the precursor used, its pretreatment and the operating conditions. The reaction has been conducted in fixed bed as well as slurry reactors at temperatures ranging from 523 to 673 K and pressures from 0.1 to 2.5 MPa, using H_2/CO_2 mole ratio varying from 1/1 to 8/1. The space velocity of the reaction mixture is also varied from 200 to 6000 cm^3 (NTP) h^{-1} g^{-1}. In spite of voluminous data available, there has been very few comprehensive reviews on the F–T synthesis carried out on Fe-based catalysts.

The present review deals with the work carried out on the F–T synthesis, by carbon dioxide hydrogenation, on Fe based catalysts. The objective of the present review is to highlight the progress made in our group on the catalyst development and the efforts put forth in achieving high conversion and product selectivity.

2 Experimental

2.1 Catalyst Preparation

The general procedure for the preparation of co-precipitated Fe–Cu, Fe–Cu–Al and metal, M (M = V, Cr, Mn and Zn) promoted iron catalysts was as follows. The required quantities of aqueous metal nitrate solutions were first mixed and then precipitated with an aqueous solution of NH_4OH (10 wt.%) at pH 7. The co-precipitated materials were initially filtered, washed with distilled water, dried at 383 K for 24 h and finally calcined at 723 K for 5 h. The Fe:M atomic ratio of the promoted catalysts was kept at 9/1. In the case of Zn promoted iron catalysts, the Zn/Fe atomic ratio was also varied in the region of 0–1.0.

The preparation of Fe–Cu–K catalyst involved two steps: preparation of Fe–Cu precursor by co-precipitation, followed by impregnation of the precursor with potassium carbonate, adopting the incipient wetness technique. In the case of Fe–Cu–Al–K and Fe–Cu–Si–K the introduction of the structural promoter, Al_2O_3 or SiO_2, was realized by physical mixing of the washed precipitate with colloidal SiO_2 or colloidal Al_2O_3. For one batch, the Fe–Cu–Al precursor was prepared by continuous co-precipitation using aluminium nitrate along with the other two metal nitrate solutions. The procedures for potassium addition and drying, as well as calcination, were the same as mentioned above. For the preparation of Fe–Cu–Al–K catalysts, with varying K loading, the amount of potassium carbonate added was varied as per the requirement. The compositions of the individual catalysts are mentioned at appropriate places in the text of this manuscript. In the case of catalysts prepared by decomposition, the homogeneous mixture of $Fe(NO_3)_3 \cdot 9H_2O$ and K_2CO_3 was decomposed at 773 K.

Supported iron oxide catalysts with variable iron loading were prepared by impregnating γ-Al_2O_3 (Strem, 157 m^2/g) with appropriate amounts of aqueous solutions of $Fe(NO_3)_3 \cdot 9H_2O$. To prepare the supported iron-potassium catalysts with different ratios of K/Fe, in the molar ratio of 0–1.0, adequate amounts of K_2CO_3 were added to the aqueous solution of $Fe(NO_3)_3 \cdot 9H_2O$ before impregnation. After the impregnation of the support, the catalyst samples were dried at 383 K for 24 h and calcined in air at 773 K overnight.

For the synthesis of alkali modified zeolites the following procedure was adopted. The zeolite NaY (Si/Al atomic ratio: 2.43) was synthesized according to the procedure described in the literature [11]. The hydrogen form of the Y zeolite was obtained by ion exchange of the Na-form with NH_4^+ and subsequent decomposition of the ammonium form by calcination. The cation-exchanged Y zeolite samples were prepared by exchange with the alkali metal ions Li, Na, K, Rb; using an excess of 10 vol.% aqueous nitrate solutions, at 353 K. The ion-exchanged zeolite Y samples were impregnated using aqueous solutions of iron nitrate to obtain the NaY-supported Fe catalysts (17 wt.% of Fe). All catalyst samples were dried at 383 K and calcined in air at 773 K for 24 h.

2.2 Catalyst Characterization

The BET surface area and pore volume of the samples were measured by nitrogen adsorption/desorption at 77 K on a Micromeritics (ASAP 2400) instrument. Powder X-ray diffraction patterns were recorded on a Rigaku D/MAX III B diffractometer with a copper target. The chemical compositions of the samples were determined by using a Shimadzu ICP-AES (ICPS-1000 III). X-ray photoelectron spectroscopy (XPS) measurements of the catalysts were carried out with a VG Escalab MK II photoelectron spectrometer, which was equipped with a magnesium anode operated at 15 kV and 20 mA. Mossbauer spectra of the catalysts were recorded at room temperature using the spectrometer equipped with a 308 channel pulsed height analyzer. The source used for this study was ^{57}Co in Rh matrix in the standard transmission geometry.

For temperature programmed reduction (TPR) experiments, the catalyst samples were first activated in a He flow at 673 K for 1 h, followed by cooling to 323 K. A gas mixture of 5% H_2/argon was passed over the samples at a flow rate of 30 mL/min. The temperature of the samples was increased linearly at a rate of 10 K/min. Any water which formed during the reduction was trapped by a molecular sieve. The hydrogen consumption was continuously monitored by a thermal conductivity detector. For comparison, the TPR experiments of pure CuO and Cu_2O reagents were carried out in the same way.

For CO_2 temperature programmed desorption (TPD), the catalyst samples were first reduced in a 10% H_2/N_2 mixture for 3 h at 523 K, followed by exposing to excess quantity of CO_2 at 298 K. Desorption was then performed by increasing the temperature from 298 to 873 K at a rate of 10 K/min and maintained at 873 K for 1 h under a flow of helium. The CO_2 and H_2 uptakes of the catalysts were obtained at 308 K using the chemisorption apparatus (Micromeritics ASAP 2000). The samples used in the chemisorption studies were reduced for 13 h at 573 K in a flow of hydrogen, evacuated at the reduction temperature and then cooled to the adsorption temperature. From the isotherms, the CO_2 and H_2 uptakes were calculated by extending the isotherms to zero pressure. The difference between the adsorption isotherms obtained by the repeated use of gas dosing and degassing system gave the amount of chemisorbed gas on the catalysts.

2.3 Catalytic Activity Test

For evaluation in a fixed bed reactor, the catalyst was reduced in hydrogen at 723 K for 24 h. For one typical run, the reaction was started at 573 K with a feed ratio of CO_2:H_2 of 1:3 at a space velocity of 1800 mL/(g_{cat} h) under the pressure of 1–2 MPa. Ar was used as an internal standard for gas chromatographic (GC) analysis. The reactor effluent was periodically analyzed in an on-line GC (Donam DS 6200). Ar, CO_2, CO and CH_4 were analyzed by a TCD, with a carbosphere column, while light hydrocarbons (C_1–C_8) were analyzed by a FID with a GS-Q capillary column.

3 Results and Discussion

3.1 Studies on Bulk Catalysts

3.1.1 Effect of Al_2O_3 or SiO_2 as a Structural Promoter

The changes in the structure and carbon dioxide hydrogenation functionality of Fe–Cu–K catalysts were studied [12] before and after the addition of Al_2O_3 or SiO_2 as structural promoter. When the promoters were added first by physical mixing, the specific surface area and pore volume of the catalysts increased (Table 1). Whereas Al_2O_3 caused increase in CO_2 uptake (328 μmol/g against 67 μmol/g of unsupported catalyst) and a decrease in H_2 uptake (3.2 μmol/g against 21.4 μmol/g of unsupported catalyst), SiO_2 decreased both of them (12.5 for CO_2 and 6.5 μmol/g for H_2, respectively). Physically mixed catalysts had limited advantage in terms of conversion and selectivity. The catalyst prepared by adding Al_2O_3 during co-precipitation, increased the CO_2 uptake (425 μmol/g). In the case of promoted iron catalysts, it was observed that H_2 chemisorbed only on Fe, whereas CO_2 chemisorbed on both Fe and K. Al_2O_3 increased the dispersion of Fe whereas SiO_2 decreased it, the later due to poor contact between Fe and K as also reported in the literature [13]. The TPR profile of the co-precipitated Fe–Cu–Al–K catalyst also showed sharper peak for the reduction of Fe indicating better exposure of the metal. Enhancement in the CO_2 hydrogenation activity and decrease in CO selectivity were noticed for this catalyst. It is widely recognized that iron is the active component for

Table 1 Characteristics and reactivity of Fe–Cu–K catalysts before and after the addition of Al_2O_3 or SiO_2 as structural promoter [12]

Catalyst	BET S.A. (m^2/g)	Pore vol. (cc/g)	CO_2 conv. (%)	Products selectivity (%)						O/P	
				CO	CH_4	C_2	C_3	C_4	C_{5+}	C_2	C_4
Fe–Cu–K 100:6.6:4	10	0.09	10.8	39.3	9.1	7.5	9.5	7.6	26.9	2.71	2.83
Fe–Cu–Al–K 100:6.6:15.7:4	88	0.18	11.3	45.0	8.5	6.0	7.5	5.9	27.1	1.08	2.54
Fe–Cu–Si–K 100:6.6:15.7:4	257	0.48	10.2	43.4	21.1	7.6	10.5	8.5	8.8	0.03	0.14
Fe–Cu–Al–K(2) 100:6.6:15.7:4	139	0.20	15.6	22.8	9.9	7.9	11.3	8.6	39.4	0.47	1.74

RWGS and F–T reactions and the increase in iron surface area increases CO_2 conversion.

3.1.2 *Influence of Potassium*

In the case of co-precipitated iron catalysts, with their Fe:Cu:Al:K ratios varying as 100:6.6:15.7:2–8, an increase in K content increased BET surface area due to increase in dispersion [12], reaching a maximum at a Fe/K ratio of 100/6 (w/w). An examination of the surface composition of the various species on the catalyst revealed that the order of proximity of K to the other elements was in the order Cu > Fe > Al [12]. With increase in the K loading the CO_2 uptake increased and the H_2 uptake decreased, as reported in the case of impregnated Fe–K/Al_2O_3 catalysts [14]. The TPR profiles indicated the two-step reduction mechanism of Fe_2O_3; i.e., $Fe_2O_3 \rightarrow Fe_3O_4 \rightarrow Fe$. With the increase in K concentration, the first peak shifted gradually towards higher temperature and the starting point of the second peak moved to lower temperature, which meant that potassium addition led to the retardation of the initial reduction, but facilitation of reduction of Fe_3O_4 to Fe.

Table 2 shows the results of CO_2 hydrogenation over the precipitated Fe–Cu–Al–K catalysts with different K loading. Unpromoted Fe–Cu–Al catalyst showed a good CO_2 conversion. However, the selectivity to CO and CH_4 accounted for more than 60% and C_1 to C_4 constituted more than 85%. With the increase of K content from K/Fe ratio of 2/100 to 6/100, CO_2 conversion increased monotonously, while CO and CH_4 selectivity showed a reverse trend. Further increase in K loading led to decrease in CO_2 conversion and increase in CO selectivity. It can be found from Table 2 that both C_{5+} selectivity (except for Fe–Cu–Al–K(4)) and O/P ratio increased, while C_1 selectivity decreased with increasing K loading. K being a base enhanced both the strength and coverage of CO_2 adsorption on the catalyst surface leading to enhanced CO coverage and in turn, the F–T synthesis activity, in terms of chain propagation. A simultaneous decrease in the H_2 adsorption capacity led to decrease in paraffin selectivity.

3.1.3 *Studies on V, Cr, Mn and Zn Promoted Iron Catalysts*

The study was aimed at understanding the promotional effects of V, Cr, Mn and Zn on Fe [15]. The catalysts were prepared by co-precipitation method with the atomic ratio of Fe to promoted metal as 9:1. Zn promoted iron catalysts were prepared with different Zn/Fe atomic ratios in the

Table 2 CO_2 hydrogenation results over the Fe–Cu–Al–K catalysis with different potassium loading [12]

Catalysis	CO_2 conv. (%)	Product selectivity (C mol%)						O/P ratio		
		CO	Hydrocarbons							
			CH_4	C_2	C_3	C_4	C_{5+}	C_2	C_3	C_4
Fe–Cu–Al	13.1	35.5	28.2	11.0	10.8	6.4	8.0	0.01	0.12	0.16
Fe–Cu–Al–K(1)	13.2	28.0	16.3	9.6	11.7	7.1	27.2	0.06	0.61	0.50
Fe–Cu–Al–K(2)	15.6	22.8	9.9	7.9	11.3	8.6	39.4	0.47	2.17	1.74
Fe–Cu–Al–K(3)	16.9	18.0	9.4	7.3	10.4	7.5	47.3	1.16	2.68	2.39
Fe–Cu–Al–K(4)	14.4	20.9	8.7	7.4	10.2	7.9	44.8	2.14	7.27	3.20

Reaction conditions; T = 538 K, $P_{CO_2+H_2}$ = 1.27 MPa, W/F = 10 g_{cat} h/mol(CO_2 + H_2), H_2/CO_2 = 3

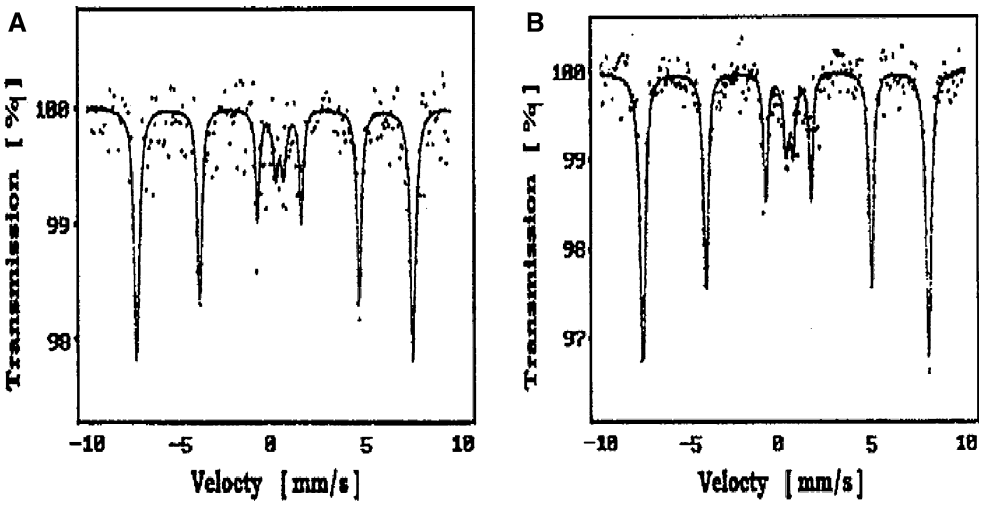

Fig. 1 Mossbauer spectra of the promoted iron catalysts at room temperature [15]. (**a**) Fresh V–Fe, (**b**) fresh Zn–Fe (the wt. ratio of M:Fe is 10:90)

Table 3 CO_2 hydrogenation on various co-precipitated iron–metal catalysts[a] [15]

Catalysts (Fe–M)	CO_2 conv. (%)	Selectivity (C mol%)		Hydrocarbon distribution (C mol%)								O (%)[b] (O + P)
		CO	HC	C_1	$C_2^=$	C_2	$C_3^=$	C_3	$C_4^=$	C_4	C_5>	C_2–C_4
Fe	16.21	36.39	63.61	49.67	0.24	16.26	1.17	16.61	1.15	7.51	4.41	5.55
Fe–V	11.17	27.30	72.70	39.72	1.57	15.02	–	22.05	5.88	8.22	7.54	14.13
Fe–Cr	25.70	21.53	78.47	64.75	1.01	15.54	4.05	7.39	2.10	2.91	2.25	21.70
Fe–Mn	23.15	8.06	91.94	38.06	1.24	17.42	8.00	13.82	5.09	8.84	7.53	26.34
Fe–Zn	26.54	4.35	95.65	24.26	6.95	7.11	19.58	4.92	13.93	5.60	17.29	69.64

[a] CO_2 hydrogenation at 1900 mL/g/h, 573 K, and 0.1 MPa

[b] Selectivity to olefins(C mol%)

range of 0–1.0. The XRD and the Mossbauer spectroscopic analyses of fresh catalysts showed formation of α-Fe_2O_3 phase in the form of large particles in an amorphous matrix. The Mossbauer spectra (Fig. 1) also showed superposition of patterns for iron carbides and high-spin Fe^{3+} ions. A greater proportion of catalyst was found be to be covered with carbon containing species (Fe_xC_y [x,y:integer]: The amount of chemisorbed carbon dioxide increased in the order of V < Cr < Mn < Zn).

Hydrogenation of carbon dioxide (Table 3) carried out in a continuous fixed bed flow reactor over these catalysts gave the following results. The products followed Anderson–Schultz–Flory distribution. The addition of V to Fe easily oxidized the catalyst surface and prevented its transformation to iron carbide species, decreasing the conversion of carbon dioxide and there was no advantage to the selectivity to C_2–C_4 alkenes. Cr, Mn and Zn, on the other hand, generated more basic iron carbide species thus increasing the selectivity to C_2–C_4 alkenes. The acidic carbon dioxide favored the basic sites of catalyst surface for chemisorption, and enhanced the formation of hydrocarbons. The possibility of chain growth increased with increase in the number of active sites. Zn promotion further increased the selectivity to C_2–C_4 alkenes, especially the light olefins. CO_2 chemisorption uptake experiments revealed that this value varied in the order V < Cr < Mn < Zn. Thus, Zn acted as a base which preferably adsorbed and activated carbon dioxide. The readsorption of olefins was also retarded by the presence of strongly adsorbed CO_2. The catalyst with a Fe:Zn ratio of 90:10 showed the highest conversion of carbon dioxide, and highest selectivity for olefin formation.

3.1.4 The Episodes of F–T Regime Formation and Construction of the Catalyst [16]

Generally the fresh iron catalysts used for the F–T synthesis take some time to achieve steady-state [17] because the reduced catalyst undergoes several transformations under the influence of reaction medium associated with considerable change in the product distribution. Thus, for the 'construction' of the actual catalyst, it is necessary to understand these changes and correlate them with activity and selectivity. The progress of the work done in this direction is illustrated below. By means of collecting the catalysts as well as product samples at definite intervals of time, investigations were carried out to establish the different reaction regimes.

During episode I, which occurred in the first seven minutes of the reaction, there was high CO_2 consumption due to surface coverage leading to sufficient amount of carbon retained on the catalyst. No formation of hydrocarbons was observed as there was no F–T activity. This was where iron as a F–T catalyst differed fundamentally from the other F–T catalysts like Co, Ru and Ni. The products of reverse water gas shift reaction were progressively obtained from the H_2/CO_2-syngas during episode II. More CO was formed from CO_2 than consumed for carbiding. However, the F–T activity was still (almost) zero. In episode III, the (reverse) water gas shift activity developed further, whereas carbiding declined. At the end of episode III the carbiding of the catalyst was completed (pseudo-steady low level). The RWGS-yield showed a maximum in the beginning of episode IV with increasing the F–T yield. During episode V, the faster consumption of CO by the F–T reaction caused the lowering of CO-yield. The F–T activity picked up and achieved its maximum. In the final episode VI, the deactivation of the catalyst was observed. In the case of CO_2 hydrogenation, the time of construction of catalyst took very long time, as for example, in some cases about 5000 min, because of much less CO being available for carbiding the iron. With increase in the extent of alkali loading, a higher steady state F–T activity and higher yield of F–T hydrocarbons were observed. The high degree of alkalization was beneficial for F–T synthesis with the H_2/CO_2-syngas. In general, it was concluded that F–T synthesis with a H_2/CO_2-syngas is feasible on highly alkalized iron catalysts.

3.1.5 *Surface Polymerization Model and the Description of Chain Growth and Branching*

On the basis of a "non-trivial surface polymerization" model, the product composition (selectivity) was described, for many individual compounds and their kinetic coefficients evaluated. The reaction probabilities of adsorbed intermediates were worked out for explaining the chain growth probability, α; chain branching and desorption as olefin or paraffin. The basic model was extended to reaction reversibility, secondary reactions (as for olefins) or oxygenates formation [18], whenever necessary.

For two catalysts with different alkali contents, the α value was found to depend on the composition of the synthesis gas and also the extent of alkali loading. An increase of growth probability (from ca. 0.6 to ca. 0.78–0.82) with carbon number (Nc) was noticed in the range Nc = 3 to Nc = 10. This was explained by readsorption of olefins on F–T sites for further chain growth. The experimental data on the reactivity of catalysts at different times on stream [16] revealed that up to steady-state the curves of growth probability were much the same. The increase of α with carbon number resulted mainly from increasing reactor residence time [18]. It was concluded that the transformation of the fresh Fe containing F–T catalyst into its active form meant essentially increasing the number of F–T sites of the same kind.

Branching (as expressed in terms of producing a tertiary C-atom in the growing aliphatic chain) was more demanding in space than linear chain prolongation, forming only secondary C-atoms. It was expected that larger species need more space for the branching reaction transition-state. The normal assumption that the probability for desorption after branching, for linear and non-linear molecules, is the same was found to be not true. The run length had essentially no influence on chain branching probability. However, the spatial constraints were lower at lower degree of alkalization. Increasing temperature reduced spatial constraints and correspondingly higher concentrations of branched compounds could be found in products on iron catalysts. The desorption of alkyl species via beta-H-abstraction was found to be about 70–80% for olefins whereas that for paraffins via H-addition was 20–30%. This desorption ratio was amazingly unaffected by reaction conditions and nature of the catalyst. The origin of oxygenates formation was also explained.

3.1.6 *Compositional and Structural Changes in the Catalyst During the Episodes*

The characteristics of the catalysts were examined at each stage (episode), and some of them are given below. The BET surface area (34 m^2/g) and pore volume (0.14 cm^3/g) of the catalyst remained almost constant during episodes I to IV and showed a drastic decrease during episode V (2 m^2/g and 0.015 cm^3/g, respectively) due to accumulation of wax formed as a product. Inspection of the catalyst samples by Mossbauer spectroscopy [16] yielded interesting results about the changes in iron containing phases. The composition of Fe-phase did not change during the episodes I, II and III. But in episode IV, when the F–T activity was being created, there was consumption of the α-Fe and the respective formation of the Fe_5C_2-carbide until all the metallic iron was consumed. At steady state activity, the Fe_2O_3 phase disappeared almost completely and the amount of the magnetite phase shrunk drastically, whereas that of the "unknown" oxidic iron phase increased. This phase was considered responsible for the reverse water gas shift reaction, as it was supposed to provide hydrogen dissociation and spill over to the carbide phase. A principal conclusion was that the metallic iron was not active as F–T catalyst. The F–T activity related to the Fe_5C_2 iron carbide phase. The actual F–T sites were expected to be established under the influence of surface species as H, C, CH_x, C_xH_y, OH, CO at distinct partial pressures of H_2, CO, H_2O and CO_2 and

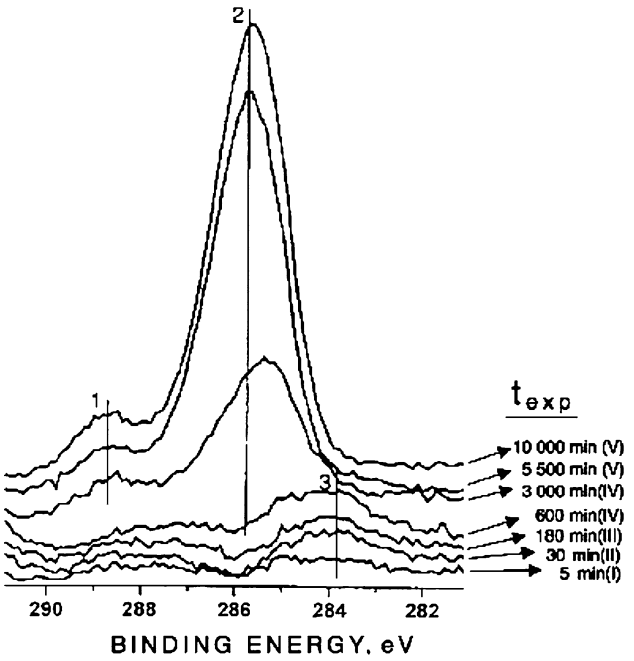

Fig. 2 XPS peaks of surface carbon (C-1s electrons) on iron Fischer–Tropsch catalysts used for different run lengths [16]. Peak assignment (tentative): peak 1 at 288.8 eV; carbonate carbon peak 2 at 285.7 eV; carbonaceous and organic carbon peak 3 at 283.9 eV; carbidic carbon FT conditions: $H_2/CO_2 = 3$, Fe–Al–Cu–9K, 523 K, 1 MPa, 30 cm^3 (NTP)/min and g (Fe). Peak assignment: 1, carbonate carbon (288.8 eV); 2, deposited carbon, organic (285.7 eV); 3, carbidic carbon (285.7 eV)

obviously substantially modified by the alkali promoter. The spill over hydrogen from the unknown iron phase reacts with this carbide phase leading to F–T hydrocarbon formation.

From the XPS analysis of the catalysts the following points were arrived at. The K/Fe atomic surface ratio increased drastically from a value of ca. 3 to a value of almost 20, indicating that K migrated from bulk to surface with restructuring of the bulk iron phase. By means of the increasing areas of the two peaks (Fig. 2) corresponding to the carbon from non-volatile organic products and the carbonate carbon, which appeared in the binding energy range 280–300 eV, the XPS-results also corroborated the high K/Fe-atomic surface ratio at long run lengths and with the amorphous oxidic Fe-phase formation.

3.1.7 The Effect of H_2O and CO_2 on the Activities of Fe Catalysts

H_2O in the reacting mixture strongly inhibits the reaction kinetics, thereby reducing the possibility of attaining high syngas conversion per pass. Both H_2O and CO_2 are oxidising compounds in the reacting mixture and may cause oxidation and structural changes of the iron catalyst [19]. Low CO partial pressure decreases its carbiding potential. In the case of cobalt catalysts, the presence of H_2O can be beneficial as it substantially reduces methane selectivity.

3.1.8 The Formation of Different Iron Carbides

During the CO_2 hydrogenation on Fe catalysts the formation of χ-Fe_5C_2, Θ-Fe_3C and Fe_3O_4 phases were observed [20]. Lee et al. [3] also disclosed that the carbide formation was favored by K-promotion. Fe_2O_3 rapidly transformed to Fe_3O_4 and then slowly to χ-Fe_5C_2. However, metallic iron transformed to ε'-$Fe_{2,2}C$ and χ-Fe_5C_2 and with supported iron catalysts, the carbide phase mainly consisted of χ-Fe_5C_2 [21]. A strong interrelation between iron carbide formation and catalyst F–T activity for CO_2 hydrogenation was reported by Fiato et al. [5].

3.1.9 The Influence of CO_2 Composition in CO–CO_2 Mixture on the Hydrogenation Reaction Over Fe/K/Al/Cu Catalyst

The influence of CO_2 composition in the mixture of CO and CO_2 during the hydrogenation was studied in detail in order to obtain a comparative account of the reactivities on Fe and Co catalysts. The yield of organic compounds decreased, to a much lower degree with increasing CO_2 molar fraction of the synthesis gas, as in case of the Co catalyst. Conversion of CO was preferred up to the molar CO_2 content of 0.5. The product distribution obtained during CO or CO_2 hydrogenation was the same on Fe catalysts, which was remarkable. When compared to those obtained with the Co catalyst, the chain growth probabilities observed on Fe catalysts, for the two reactions were also the same for synthesis gases having the same composition of $H_2/CO = 2.3$ and $H_2/CO_2 = 2.3$. This showed that neither methane formation nor chain growth was controlled by the partial pressure of CO in the case of a F–T regime with iron catalysts. These results are disclosed in detail by Riedel et al. [22].

3.2 Supported Fe–K Catalysts

3.2.1 The Influence of Fe/K Ratio

Hydrogenation of CO_2 was carried out on Al_2O_3-supported Fe–K catalysts [13]. With a constant iron loading, the K/Fe molar ratio was varied in the range 0–1.0. The CO_2 chemisorption capacity enhanced remarkably whereas that of H_2 diminished by the addition of K to the $Fe/A1_2O_3$ catalyst. The increase in CO_2 chemisorption was due to increase in surface basicity and it was also apparent that H_2 was adsorbed on only Fe but CO_2 adsorbed on both Fe and K. From the sequential adsorption studies it was noticed that pre-chemisorption of H_2 could not reduce the chemisorption of CO_2 in the second adsorption and vice versa (Table 4). This suggested that the active site for one gas was different from that for the other gas. From the

Table 4 The chemisorbed amounts of H_2 and CO_2 on Fe/alumina and K–Fe/alumina catalysts [13]

K/Fe atomic ratio	$H_2 \rightarrow CO_2$[a]		$CO_2 \rightarrow H_2$[b]	
	H_2 uptake (μmol/g)	CO_2 uptake (μmol/g)	CO_2 uptake (μmol/g)	H_2 uptake (μmol/g)
0.0	31.0	169	167	34.8
0.2	26.4	305	290(307)[c]	30.2
0.5	20.1	533	514(509)	25.6
1.0	8.5	398	376(379)	5.3

[a] The order of sequential adsorption was H_2 and CO_2

[b] The order of sequential adsorption was CO_2 and H_2

[c] Numbers in the parentheses indicate the results with K/alumina samples which contain the same amounts of K as K–Fe/alumina samples

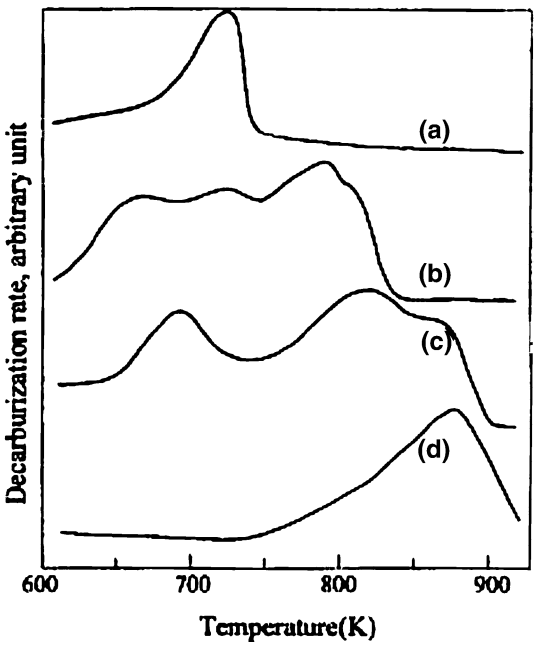

Fig. 3 Temperature programmed decarburization of carbides on the catalyst surface [13]. (a) Fe/Al_2O_3, (b) $Fe–K/Al_2O_3$ (K/Fe = 0.2), (c) $Fe–K/Al_2O_3$ (K/Fe = 0.5), (d) $Fe–K/Al_2O_3$ (K/Fe = 1.0)

temperature programmed decarburization (TPDC) studies it was found that K increased the stability of surface carbides on the catalyst as revealed by the high temperature shift (Fig. 3) of the decarburization profiles on the potassium containing catalysts. Table 5 illustrates the catalytic activity performed in a continuous fixed bed reactor at 573 K and 2 MPa pressure as a function of potassium content. The CO_2 conversion and yield of hydrocarbons increased upto K/Fe = 0.5 and then on decreased slightly. Further, the selectivities towards C_{2+} hydrocarbons and light olefins increased with increasing potassium content.

3.2.2 *The Effect of Pressure on the Reaction*

The formation of hydrocarbons from CO_2 takes place via the two-step mechanism involving the reverse water–gas shift (RWGS) reaction and the F–T reaction [22]. Information about the RWGS reaction on the catalysts was obtained at atmospheric pressure. The results on Fe/Al_2O_3 and $Fe–K/Al_2O_3$ catalysts at 573 K showed higher selectivity towards CO as compared to the reactions at 2 MPa. The higher activity of $Fe–K/Al_2O_3$ catalysts for the RWGS reaction contributed to the increase in the C_{2+} hydrocarbon formation from carbon dioxide at the elevated pressure. The activity and selectivity data obtained at 673 K and 2 MPa revealed that the distribution of hydrocarbons strongly depended on the potassium content as the selectivity to methane in hydrocarbons decreased considerably. The chain growth probability, α, for C_3–C_5 hydrocarbons increased upto K/Fe = 0.5. This was attributed to the

Table 5 Activity data on K containing Fe/Al_2O_3 catalysts (673 K and 2 MPa) [13]

	K/Fe molar ratio			
	0	0.2	0.5	1.0
CO_2 conversion	48.9	67.3	69.6	68.4
Selectivity (C mol%)				
CO	12.4	6.0	3.9	4.5
Hydrocarbons	87.6	94.0	96.1	95.5
Hydrocarbon distribution (C mol%)				
C_1	48.4	18.3	16.7	18.2
C_2 olefin	0.3	7.8	10.2	11.5
C_2 paraffin	20.2	6.1	2.1	2.1
C_3 olefin	1.2	19.9	17.2	18.7
C_3 paraffin	16.2	2.8	1.8	1.8
C_4 olefin	1.5	11.2	13.7	13.9
C_4 paraffin	7.4	5.7	2.6	0.5
C_5	3.8	13.7	16.3	16.1
C_{6+}	0.9	14.5	16.5	17.2
STY(C mol/(kg h))hydrocarbons	9.0	13.3	14.1	13.7
Chain growth probability α[a]	0.39	0.60	0.72	0.69

[a] The chain growth probability used in Anderson–Schulz–Flory statistics

Table 6 CO_2-hydrogenation on supported Fe catalysts [22]

Catalysts	CO_2 conv. (%)	Yield (C%)		Hydrocarbon distribution (C mol%)								Olefins C_2–C_4 (mol%)
		CO	HC	C_1	$C_2^=$	C_2	$C_3^=$	C_3	$C_4^=$	C_4	C_5>	
$FeSiO_2$	6.9	4.9	2.0	80.9	–	13.7	0.12	4.5	–	1.3	0.42	0.64
Fe/TiO_2	11.5	4.1	7.4	51.7	0.07	16.7	0.57	14.9	0.51	8.8	6.8	2.70
Fe/Al_2O_3	22.8	2.6	20.2	43.2	0.02	19.1	0.15	17.9	0.11	10.8	8.8	0.58
$Fe–K/Al_2O_3$	30.4	12.3	18.1	12.7	9.7	1.8	17.0	2.1	16.9	0.28	39.4	91.3

Reaction conditions 573 K, 1.01 MPa, 31.6 mL syngas/min/g of catalyst (NTP): $H_2/CO_2 = 3$

increased ability of CO_2 chemisorption on highly K-containing catalysts than that of H_2 in the formation of C–C bond. It is known that in the F–T reaction, olefins are formed as primary products and undergo hydrogenation in the secondary steps [23] to form paraffins. The low surface concentration of hydrogen on highly K-containing catalysts would also be a favorable condition for olefin formation. This tendency of catalysts giving improved selectivity towards olefins in C_2–C_4 hydrocarbons was also correlated with the extent of carburization [24].

3.2.3 The Influence of the Nature of Support

3.2.3.1 SiO_2, TiO_2 and Al_2O_3 Supported Iron Catalysts [22] SiO_2, TiO_2 and Al_2O_3 supported iron catalysts were examined for their H_2 and CO_2 chemisorption capacities. The adsorption capacities of Fe/SiO_2 and Fe/TiO_2 were much smaller than those observed on γ-Al_2O_3 supported iron catalyst. The TPDC study displayed two types of peaks; the low temperature peak corresponding to surface carbide and the high temperature peak to bulk phase iron carbide. The stability of the carbides increased in the order Fe/γ-$Al_2O_3 < Fe/SiO_2 < Fe/TiO_2$.

Results of activity tests for CO_2 hydrogenation with the supported iron catalysts are presented in Table 6. The activity of the SiO_2 supported catalyst was the lowest, whereas that for the Al_2O_3 supported iron, the highest. With Al_2O_3 as support the yield of hydrocarbons was again about three times higher. The potassium promoted Al_2O_3 supported iron catalyst yielded a F–T typical hydrocarbon product with $\sim$13% methane and of high olefinicity.

3.2.3.2 Iron Catalysts Supported on Ion Exchanged Y-Zeolites [22] This study was carried out in two parts. In the first part HY zeolite supported Fe catalysts were prepared with varying Fe loading, characterized by several techniques and their carbon dioxide hydrogenation capacity evaluated. At low (2 and 5 wt.% Fe) loading the Fe existed in a dispersed state. Upto 17 wt.% an X-ray amorphous layer of Fe oxide covered the zeolite and beyond that loading large Fe_2O_3 crystallites were formed decreasing the dispersion. The conversion of CO_2 and the yield of hydrocarbons increased upto 20 wt.% Fe loading and then on the increase was marginal. In the second part, keeping the Fe loading constant at 17 wt.%, catalysts were prepared by modifying the support. Several ion exchanged Y zeolites were prepared by replacing Na by H and other alkali metal ions (Li, K, and Rb). The CO_2 uptake increased in the order $Li < Na < K < Rb$ with increasing basicity of the alkali metal oxides, which might be related to the influence on the local electron density of neighboring iron species [25]. The results were consistent with the explanation that CO_2 was adsorbed on the iron and also on the iron interacting with the alkali ions present in the zeolite matrix.

From the TPR studies, it was observed that in contrast to the reduction of Fe_2O_3, which proceeded in two steps, a third peak appeared for the supported catalysts. The new peak was assigned to the reduction of Fe_3O_4 to FeO. Gao et al. [26] concluded from their studies on Fe_2O_3/γ-Al_2O_3 by TPR and XRD, that FeO, compared with either Fe_3O_4 or α-Fe, was metastable at temperatures below 840 K and that FeO could hardly be detected during the reduction of Fe_2O_3 to Fe. However, the occurrence of the peak corresponding to the reduction of FeO in this study indicated that in the presence of HY, FeO could be stabilized. The TPDC profile of Fe/HY showed one peak at 783 K. When H was replaced by alkali cations a second peak appeared before the main peak indicating the presence of a second more reactive carbide species. The results were in agreement with earlier findings [27] of two carbide phases with Fe–K catalysts, which were identified as Θ-Fe_3C and χ-Fe_5C_2.

The results of catalytic tests for CO_2 hydrogenation are presented in Table 7. A relatively low conversion of CO_2 was obtained with the Fe/HY catalyst and more than 70% of the hydrocarbons consisted of methane. Alkali metals as catalyst components caused a drastic decline of the methane selectivity, accompanied by a strong increase in olefinicity of the C_2–C_4 hydrocarbons. This result was in accordance with data from Anderson [28] showing that by addition of potassium to an iron catalyst the hydrogenation of CO resulted in a decrease of CH_4 selectivity and an increase of olefinicity. These effects increased in the order of basicity of the alkali metals $Li < Na < K < Rb$, in the

Table 7 CO_2 hydrogenation on Fe/Y-zeolite catalysts [22]

Catalysts	CO_2 conv. (%)	Yield (C%)		Hydrocarbon distribution (C%)								Olefins in C_2–C_4 (mol%)
		CO	HC	C_1	$C_2^=$	C_2	$C_3^=$	C_3	C_4	$C_4^=$	C_5>	
Fe/HY	10.1	3.0	6.1	72.6	0.02	15.2	0.07	7.6	–	2.9	1.5	0.36
Fe/LiY	17.2	7.6	9.6	17.9	3.7	9.4	12.7	4.5	9.6	3.5	38.8	60.0
Fe/NaY	20.8	6.1	14.7	14.6	7.9	4.9	13.5	4.6	11.2	3.5	39.9	71.4
Fe–KY	17.9	5.6	12.3	12.5	8.9	3.2	13.0	3.2	10.4	3.8	44.5	75.9
Fe/RbY	17.2	5.4	11.8	9.5	7.1	2.2	11.6	2.4	9.8	2.7	54.4	79.6

Reaction conditions: 573 K, 1.01 MPa, 32 mL syngas/min/g of catalyst (NTP): $H_2/CO_2 = 3$

order of their increasing electron donating ability. The degree of ion exchange was almost the same for all the catalysts used.

3.3 CO_2 Hydrogenation Using Bio-Syngas

Hydrocarbon synthesis from biomass-derived syngas (bio-syngas) was investigated as a potential way to use biomass [29]. The Fischer–Tropsch reaction was carried out using $CO/CO_2/H_2/Ar$ (11/32/52/5 vol.%) mixture as a model for bio-syngas on co-precipitated Fe/Cu/K, Fe/Cu/Si/K and Fe/Cu/Al/K catalysts in a fixed bed reactor. In the case of the Fe/Cu/Al/K system, Cu addition promoted the 1st step reduction of Fe_2O_3. On the contrary, Cu did not promote the reduction of Fe_2O_3 in the Fe/Cu/Si/K system because SiO_2 addition inhibited the interaction between Fe and Cu, due to the poor dispersion of masses. These phenomena induced the poor reactivity and lower conversion of CO_2, as shown in Table 8.

The TPDC patterns of the catalysts showed that the formation of carbide decreased in the order; Fe/Cu/K > Fe/Cu/Al/K ≫ Fe/Cu/Si/K. No carbide was formed on the SiO_2-supported catalyst. On the other hand, the Al_2O_3-supported catalyst had many types of carbides. Iron carbides are known as active species for the F–T reaction.

In commercial F–T fixed bed reactors, co-precipitated Fe/Cu/Si/K catalysts have usually been employed [30]. However, the catalysts should be readjusted to CO_2-rich and H_2-deficient feed gas in case that the bio-syngas has to be used directly as a feed for hydrocarbon synthesis. For example, the catalysts should be resistant to oxidation in the presence of CO_2. On the basis of the previous studies about CO_2 hydrogenation [12], it was possible to assume that catalysts using Al_2O_3 support would be appropriate for bio-syngas reaction. From the comparison of the results, Fe/Cu/Al/K showed much higher catalytic activity (82.78% CO conversion) than Fe/Cu/Si/K (20.61% CO conversion). However, Fe/Cu/Si/K showed fairly good activity for CO/H_2 (33/67) feed in a separate reaction experiment. The dependence of a preferable support on feed gas composition seemed to be related to differences in interaction between Fe and a support. Yan et al. [12] reported that the addition of SiO_2 to Fe–Cu–K led to poor dispersion of Fe and K on SiO_2 and thereby the interaction between Fe and K was negligible.

The catalysts with various K contents were examined in the reaction of bio-syngas. K addition remarkably enhanced CO conversion, as observed previously [13]. However, the reaction test for 160 h showed that too high K promotion (K/Fe > 0.08) led to the gradual deactivation of the catalysts, due to carbon formation. It is desirable, therefore, to select a medium K promotion (i.e., K/Fe = 0.04) as an optimum catalyst composition for the reaction of bio-syngas, as shown in Fig. 4.

3.3.1 Reaction with a H_2-Supplied Bio-Syngas

As shown in Table 8 and Fig. 4 [29] only CO was converted into hydrocarbons in the reaction with the model bio-syngas. The conversion of CO_2 was restricted by the low hydrogen content, as CO_2 needed more than 3 moles of H_2 for the production of hydrocarbons. However, a balanced feed gas made by supplying H_2 enhanced the reaction rate. The reaction data are summarized in Table 9.

Table 8 Reaction results of the comparison of alumina and silica as supports for Fe/Cu/K [29]

Catalysts	Conversion (%)			Hydrocarbon distribution (C%)				Olefin selectivity (%) in C_2–C_4
	CO	CO_2	CO + CO_2	CH_3	C_2–C_4	C_5–C_7	C_{8+}	
Fe/Cu/K(100/6/4)	87.16	0.29	22.01	9.34	35.14	20.46	35.06	88.35
Fe/Cu/Al/K(100/6/16/4)	82.78	0.26	21.18	12.62	39.19	21.89	26.31	84.92
Fe/Cu/Si/K(100/6/16/4)	20.61	−1.56	4.07	46.73	42.63	9.45	1.18	77.23

Reaction conditions: $CO/CO_2/Ar/H_2$ (11/32/5/52 in vol.%), 1 MPa, 573 K and 1800 mL/(g_{cat} h)

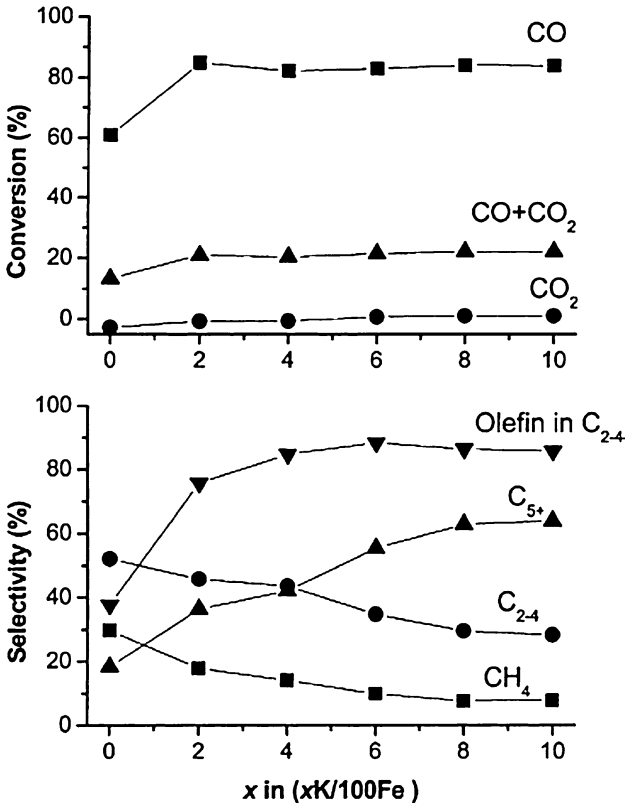

Fig. 4 Dependence of catalytic activity and selectivities on K content in Fe/Cu/Al/K (condition: $CO/CO_2/Ar/H_2$ (11/32/5/52 vol.%), 1 MPa, 573 K, GHSV = 1800 mL/(g_{cat} h)) [29]

It is apparent that the balanced feed gas resulted in much higher CO + CO_2 conversion than did the H_2-deficient feed gas and that CO_2 was converted into hydrocarbons as well as CO. As the concentration of hydrogen increases, the RWGS reaction becomes more favorable, forming more CO. High concentrations of CO, in turn, produces more hydrogenated products by F–T synthesis.

3.3.2 *Reaction with the Syngas of Various CO_2 Compositions*

In this work, the F–T reaction was also investigated with varying CO/CO_2 ratio of balanced syngas (i.e., $H_2/(2CO + 3CO_2) = 1$). The dependence of catalytic activity and selectivity on feed gas composition [29] is illustrated in Fig. 5. In the absence of CO_2, the yield of hydrocarbon was about 45% over Fe/Cu/Si/K but the yield decreased severely with increasing the $CO_2/(CO + CO_2)$ ratio. Furthermore, in the absence of CO, Fe/Cu/Si/K showed very poor hydrocarbon yield and showed very high CH_4 selectivity (>80%). Such results indicated that SiO_2 was a very poor binder in the system of Fe/Cu/K for F–T synthesis from bio-syngas. On the contrary, both Fe/Cu/K and Fe/Cu/Al/K catalysts exhibited rather high hydrocarbon yield. Both systems also showed low CH_4 selectivity and high olefin selectivity in C_2–C_4 hydrocarbons. Indeed, the F–T commercial catalysts often require binders or structural modifiers. Therefore, it was confirmed that Al_2O_3 could be a good candidate as a binder in the system of Fe/Cu/K for the F–T synthesis in the presence of CO_2.

3.4 Deactivation Studies on Fe–K/Al_2O_3 Catalyst in CO_2 Hydrogenation

3.4.1 *Studies on Impregnated Catalyst*

Catalyst deactivation in CO hydrogenation was believed to occur by phase change (Fe_3O_4 formation), sintering, fouling (coke/carbon deposit) or S poisoning [30]. As no such information was available on CO_2 hydrogenation carried out on iron based catalysts, an attempt was made for the first time in our laboratory [31] to elucidate the deactivation mechanism. To start with, an Fe–K–Al catalyst was prepared by the impregnation of γ-Al_2O_3 with aqueous solutions of $Fe(NO_3)_3 \cdot 9H_2O$ and K_2CO_3, such that the finished catalyst had the composition: 1Fe/0.35 K/5Al_2O_3 on a mass basis. The reactions were performed in a continuous fixed bed reactor at 573 K, with a feed ratio of H_2:CO_2 (3:1) and at space velocity of 1800 mL/(g_{cat} h).

Table 10 describes the time on stream analysis data obtained on this catalyst. Initially the activity increased slowly, reaching a maximum conversion after a time on stream of 70 h. A part of this catalyst was collected and named as activated catalyst. After 850 h of operation,

Table 9 Reaction results of the F–T synthesis with balanced syngas (H_2-supplied bio-syngas) [29]

Conversion (%)			Hydrocarbon distribution (C mol%)				Olefin selectivity (%) in C_2–C_4
CO	CO_2	CO + CO_2	CH_4	C_2–C_4	C_5–C_7	C_{8+}	
H_2-Deficient feed: CO/CO_2 = 0.33: $H_2/(2CO + 3CO_2)$ = 0.44							
82.78	0.26	21.18	12.62	39.19	21.89	26.31	84.92
Balance feed: CO/CO_2 = 0.33: $H_2/(2CO + 3CO_2)$ = 1							
88.17	28.89	43.65	13.75	37.66	22.18	26.41	84.01

Reaction conditions: Fe/Cu/Al/K (100/6/16/4), $CO/CO_2/Ar/H_2$ (6.3/19.5/5.5/69.3), 1 MPa, 573 K and 1800 mL/(g_{cat} h)

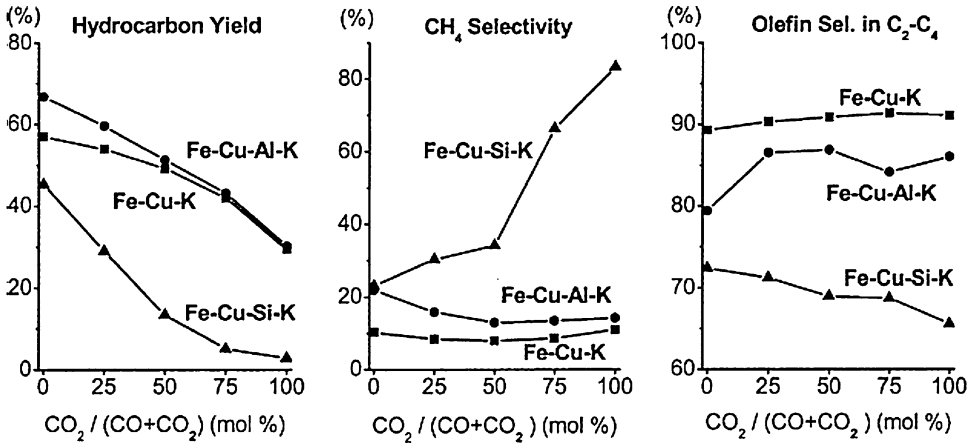

Fig. 5 Dependence of catalytic activity and selectivity on feed gas composition (balanced feed gas: $H_2/(2CO + 3CO_2) = 1$, 1 MPa, 573 K, GHSV = 1800 mL/(g_{cat} h) [29]

considerable decrease was observed in the CO_2 conversion as well as the hydrocarbon yield. The catalyst collected at this stage was named as the deactivated catalyst. The activity of the deactivated catalyst did not recover by reduction treatment, indicating that the oxidation of Fe phase was not the factor for deactivation. However, the catalytic activity was almost recovered after oxidation–reduction treatment giving an impression that the deactivation was caused mainly by the deposition of carbonaceous material. The various samples collected after different stages of treatment are designated as follows—A: activated; D: deactivated; E: extracted; R: subjected to reduction in a flow of hydrogen at 673 K and O: subjected to oxidation in a flow of air at 673 K. TGA/MS analysis revealed H_2O formation upto 443 K and then CO_2 up to 763 K. The amount of evolved CO_2 was much higher than the expected amount due to the decomposition of potassium carbonate plus CO_2 adsorbed on catalyst surface. The CO_2 uptake of the just reduced catalyst was found to be lower than that of the oxidized catalyst. If the deactivation was due to K_2CO_3 formation the uptake should have been the same. Thus, it was deduced that the deactivation of the catalyst was due to carbon or coke deposition. Since, the CO_2 uptake was higher on the oxidized sample than on the deactivated one, it was apparent that the active sites for CO_2 chemisorption on the active catalyst were covered with carbonaceous species.

From the C and H analysis and the evidence from the literature [32] the type of carbon species was identified. This result suggested that the catalyst deactivation in CO_2 hydrogenation was caused by the formation of carbonaceous material. Blocking of active sites by carbon deposites was also reported by Niemantsverdriet [33]. The Fe phase of deactivated catalyst collected after 850 h consisted of the Hägg carbide (χ-Fe_5C_2) and magnetite (Fe_3O_4), as can be seen in Fig. 6. χ-Fe_5C_2 has been known as an active phase in F–T reaction. The reduction treatment of deactivated catalyst was found to be of no use in catalyst regeneration, due to the existence of unreducible carbon, which blocks the active sites of catalyst, as evidenced by C analysis. However, oxidation followed by reduction treatment of deactivated catalyst regenerated the catalyst by removing the carbidic as well as surface carbon.

3.4.2 *Studies on Co-Precipitated Fe–Cu–K–Al Catalyst*

The deactivation study was then extended to the co-precipitated Fe–Cu–K–Al catalyst [34]. The catalyst was prepared in two steps; Fe–Cu–Al was first prepared by continuous co-precipitation method and K was

Table 10 Catalytic activity of Fe–K/alumina catalyst in CO_2 hydrogenation for long-term test and regeneration test[a] [31]

Time on stream (h)	CO_2 conv. (%)	CO yield (%)	Organic compound yield (%)	Organic compound distribution (%)				Olefin content in C_{2-4}HC (%)
				CH_4	C_{2-4}HC	C_{5-7}HC	Others	
31.0	31.33	6.99	24.34	10.69	36.29	17.43	35.59	86.31
850	25.75	10.34	15.41	14.13	40.61	13.82	31.44	85.35
After H_2-reduction treatment of the deactivated catalyst at 450 °C, 24 h								
37.8	26.39	10.35	16.04	14.64	40.78	12.67	31.91	85.07
After air-oxidation at 400 °C, 24 h, followed by H_2-reduction at 450 °C, 28 h								
40.0	30.91	6.32	24.59	12.82	38.10	15.54	34.54	84.07

[a] Conditions: 300 °C, 1 MPa and 1800 mL/(g_{cat} h), HC: hydrocarbons

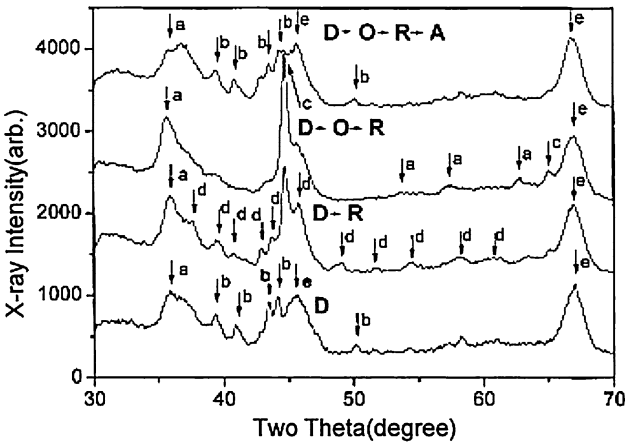

Fig. 6 XRD patterns of variously treated Fe–K/alumina catalysts [31]. D: Deactivated catalyst, O: oxidation in a flow of air at 400 °C for 12 h, R: reduction in a flow of H_2 at 673 K for 13 h, A: activation in the reaction for 74 h. (a) Fe_3O_4, (b) χ-Fe_5C_2, (c) α-Fe, (d) θ-Fe_3C, (e) γ-Al_2O_3

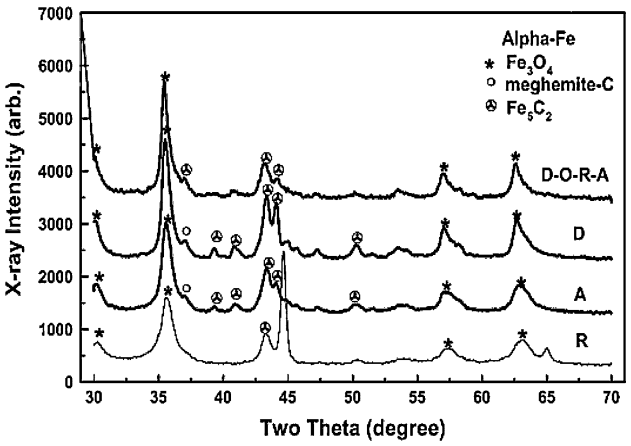

Fig. 7 XRD patterns of Fe–Cu–K–Al catalysts [34]. A: Activated catalyst (employed in the reaction for 100 h), D: deactivated catalyst (used for 2150 h), R: reduction in a flow of H_2 at 400 °C for 13 h, O: oxidation in a flow of air at 673 K for 12 h

impregnated on it using potassium carbonate. The catalyst composition was found to be 100Fe:6.6Cu:15.7Al:6K in weight ratio. The reaction was performed in a continuous fixed bed reactor with a feed ratio of CO_2:H_2 (1:3), at space velocity of 1800 mL/(g_{cat} h), under the pressure of 1 MPa. Based on the time on stream analysis, the catalyst subjected to 100 h of study was taken as the active catalyst and that tested upto 2005 h was taken as the deactivated catalyst.

The oxidation of iron phase was proposed as a dominant factor of catalyst deactivation in the reaction using CO_2-rich syngas. In this work, however, the catalytic activity of the deactivated Fe–Cu–K–Al catalyst was not recovered simply by reduction treatment. It is known that the carbidation of Fe occurs at the beginning of the reaction, consuming most of the surface-active carbon formed from CO dissociation. When the bulk phase of Fe is fully carbided, the carbonaceous materials would be deposited on the surface. Wax formed by chain growth would also be deposited in a significant amount on the catalyst through long-term reactions. Contrary to the impregnated catalyst, in the case of the co-precipitated one, even if the carbonaceous material was completely removed by oxidation treatment the catalytic activity was not recovered by the oxidation–reduction treatment. The results suggested that the carbonaceous material was not a dominant factor of the deactivation on Fe–Cu–K–Al catalyst.

The XRD analysis performed on all the samples gave some clue about the nature of deactivation. The crystallite size of iron species increased with time on stream. Although the crystallite size of the iron carbide was brought back again by the treatment of (D → O → R → A), the catalytic activity was not recovered. It was deduced that the catalyst deactivation was mainly caused by the growth of crystallite size and the resulting component separation (Fig. 7). This result was verified by the fact that the Fe_3O_4 size of (D → O → R → A) sample was bigger than that of the activated catalyst. From X-ray line broadening analysis, it was found that the crystallite size of iron oxide of the deactivated catalyst (14.3 nm) increased compared to that of the activated catalyst (9.4 nm). The corresponding values for the iron carbide also increased from 12.5 to 16.2 nm. The larger Fe species would be separated from Cu species and the Fe species without Cu promotion would be oxidized to Fe_3O_4 easily.

4 Conclusions

Potassium as a promoter decreases the selectivity to methane and increases the selectivity to C_2–C_4 hydrocarbons. It improves carburization and the chain growth probability (upto K/Fe = 0.5). Its preference for CO_2 rather than H_2 adsorption increases the probability of C-C bond formation. Iron carbides are responsible for the formation of olefins and long-chain hydrocarbons. The addition of alumina, as a structural promoter in Fe–Cu–K prepared by co-precipitation, increases the CO_2 conversion and hydrocarbon selectivity, whereas silica is unfavorable. The selectivity to olefins is improved as well as the activity and chain growth ability. By increasing the dispersion and thereby interaction between Fe and K alumina helps create more active sites for the CO_2 hydrogenation. Promotion of Fe with Cr, Mn and Zn increases the conversion of carbon dioxide. Zn increases the basicity and offers very high selectivity for C_2–C_4 alkenes.

The deactivation of the impregnated Fe–K/Al_2O_3 catalyst proceeds mainly by carbonaceous deposit formation,

whereas in the case of precipitated catalyst the deactivation is caused by the increase in crystallinity of iron species. The pathway to steady state Fischer–Tropsch synthesis on iron catalyst has been described in principle. The reduced catalyst, before synthesis, consisted of mainly α-Fe and Fe_3O_4, and small amounts of Fe_2O_3 and iron carbide. At the beginning of a synthesis run, the catalyst was (almost) not active, neither for the water–gas shift reaction (and its reverse) nor for the Fischer–Tropsch synthesis. With ongoing time, the Fe_3O_4 and Fe_2O_3 phases were consumed and a new amorphous, probably oxidic, iron phase occurred. This appears to be the ''active catalyst'' for the water–gas shift reaction, on which reversible hydrogen dissociation occurs. Simultaneously, α-Fe reacts with carbon from CO dissociation and forms iron carbide (particularly Fe_5C_2). Thus, the iron carbide surface in its "actual state during synthesis" is the "true Fischer–Tropsch catalyst". With the H_2/CO_2 syngas mild carbiding conditions prevail and only the Fe_5C_2 carbide could be detected in the used catalyst, even after a long time at the steady state of Fischer–Tropsch synthesis. Thus, the activity in the carbon dioxide hydrogenation is slow.

On the Fe based catalysts, the product selectivity at the steady state remains the same with the H_2/CO_2 and the H_2/CO syngases, in contrast with the Co based catalysts where the product composition in Fischer–Tropsch synthesis strongly depends on the partial pressures of CO and H_2. The different episodes in the path to steady-state have been delineated. The designing of the "best" Fischer–Tropsch iron catalyst demands optimization of the processes of "catalyst construction" under reaction conditions and optimum pretreatment procedures. Fe/Cu/Al/K is a suitable catalyst for F–T synthesis from bio-syngas, giving high hydrocarbon yield and olefin selectivity Fe/Cu/Si/K displays lower activity and selectivity for bio-syngas hydrogenation.

Acknowledgements The authors would like to acknowledge funding from the Korea Ministry of Commerce, Industry and Energy (MOCIE) through "Project of next-generation novel technology development" of ITEP. P.S. Sai Prasad thanks Korea Federation of Science & Technology (KOFST) for the award of the visiting research fellowship under Brain Pool program and the Director, IICT, Hyderabad, for sanctioning the sabbatical leave. K.W. Jun thanks all the co-authors of his papers cited in this review.

References

1. Edwards JH (1995) Catal Today 23:59
2. Fujimoto K, Shikada T (1987) Appl Catal 31:13
3. Lee JF, Chern WS, Lee MD, Dong TY (1992) Can J Chem Eng 70:511
4. Fujiwara M, Kieffer R, Ando H, Souma Y (1995) Appl Catal A 121:113
5. Fiato RA, Iglesia E, Rice GW, Soled SL (1998) Stud Surf Sci Catal 107:339
6. Omae I (2006) Catal Today 115:33
7. Newsome DS (1980) Catal Rev Sci Eng 21:275
8. Dry ME (1996) Appl Catal A 138:319
9. Jin Y, Datye A (2000) J Catal 196:8
10. Miller D, Moskovits M (1989) J Am Chem Soc 111:9250
11. US Patent 3,130,009, 1970
12. Yan SR, Jun KW, Hong JS, Choi MJ, Lee KW (2000) Appl Catal A 194–195:63
13. Choi PH, Jun KW, Lee SJ, Choi MJ, Lee KW (1996) Catal Lett 40:115
14. Jun KW, Lee SJ, Kim H, Choi MJ, Lee KW (1998) Stud Surf Sci Catal 114:345
15. Nam SS, Lee SJ, Kim H, Jun KW, Choi MJ, Lee KW (1997) Energy Convers Manage 38(Suppl):S397
16. Riedel T, Schulz H, Schaub G, Jun KW, Hwang JS, Lee KW (2003) Topics Catal 26:41
17. Storch HH, Golumbic N, Anderson RB (1951) The Fischer–Tropsch and related syntheses. John Wiley & Sons, New York
18. Schulz H, Claeys M (1999) Appl Catal A 186:71
19. Satterfield CN, Hanlon RT, Tung SE, Zou Z, Papaefthymiou GC (1986) Ind Eng Chem Prod Res Dev 25:407
20. Schulz H, Riedel T, Schaub G (2005) Topics Catal 32:117
21. Raupp GB, Delgass WN (1979) J Catal 58:361
22. Riedel T, Claeys M, Schulz H, Schaub G, Nam SS, Jun KW, Choi MJ, Kishan G, Lee KW (1999) Appl Catal A 186:201
23. Falconer JL, Zagli AE (1980) J Catal 62:280
24. Dictor RA, Bell AT (1986) J Catal 97:121
25. Bonzel HP, Krebs HJ (1982) Surf Sci 117:639
26. Gao X, Shen J, Hsia Y, Chen Y (1993) J Chem Soc, Faraday Trans 89:1079
27. Lee MD, Lee JF, Chang CS (1989) Bull Chem Soc Jpn 62:2756
28. Anderson RB (1984) The Fischer–Tropsch synthesis. Academic Press, London
29. Jun KW, Roh HS, Kim KS, Ryu JS, Lee KW (2004) Appl Catal A 259:221
30. Dry ME (1981) In: Anderson JR, Boudart M (eds) Catalysis science and technology, vol 1. Springer-Verlag, Berlin, p 159
31. Hwang JS, Jun KW, Lee KW (2001) Appl Catal A 208:217
32. Shultz JF, Hall WK, Dubs TA, Anderson RB (1956) J Am Chem Soc 78:282
33. Niemantsverdriet J, van der Kraan A, van Dijk W, van der Baan H (1980) J Phys Chem 84:3363
34. Hong JS, Hwang JS, Jun KW, Sur JC, Lee KW (2001) Appl Catal A 218:53